

A Control Framework to Generate Nonenergy-Storing Virtual Fixtures: Use of Simulated Plasticity

Ryo Kikuuwe, *Member, IEEE*, Naoyuki Takesue, *Member, IEEE*, and Hideo Fujimoto

Abstract—Some recent studies have addressed a class of human-machine coordination employing “virtual fixtures,” which are computer-generated walls or guides presented through haptic devices for assisting precise path tracing and for preventing the entry to specified regions. This paper presents the concept and control algorithms of a new class of virtual fixtures that is based on simulated plasticity. The plasticity-based virtual fixtures act as hard walls as long as the user’s force is smaller than a predetermined yield force, but the user can deviate from the fixtures by intentionally producing a force larger than the yield force. As a characteristic of plasticity, the proposed virtual fixtures do not store elastic energy; the reaction force from the fixture almost always opposes the user’s motion to decelerate the motion. Thus, the plasticity-based virtual fixtures are expected to be useful in some applications where safety is an utmost priority. This paper presents control algorithms for realizing the concept of plasticity-based virtual fixtures, addressing technical challenges in treating discontinuous nature of plasticity in discrete-time systems. The algorithms were demonstrated through experiments using impedance-type and admittance-type haptic devices.

Index Terms—Admittance control, energy storage, haptic rendering, impedance control, plasticity, virtual fixtures.

I. INTRODUCTION

HUMANS are capable of intelligent and dexterous manual manipulation, but human voluntary motions are generally inaccurate due to low-frequency fluctuations such as physiological tremors. One approach for enhancing the accuracy of human manual tasks is the use of a haptic device for producing some appropriate physical constraints in such a manner as illustrated in Fig. 1. In this approach, the haptic device can act like a ruler to draw a straight line or a wall to keep the tool away from some area that should not be entered. It is technically straightforward to produce such artificial constraints in telemanipulation systems. These kinds of computer-generated physical constraints are recently referred to as *virtual fixtures*. Various types of virtual fixtures have been studied for assisting telemanipulation [2]–[9]

Manuscript received May 2, 2007; revised December 19, 2007. This paper was recommended for publication by Associate Editor H. R. Choi and Editor K. Lynch upon evaluation of the reviewers’ comments. This paper was presented in part at the IEEE International Conference on Robotics and Automation, Rome, Italy, April 2007.

R. Kikuuwe is with the Department of Mechanical Engineering, Faculty of Engineering, Kyushu University, Fukuoka 819-0395, Japan (e-mail: kikuuwe@ieee.org).

N. Takesue is with the Faculty of System Design, Tokyo Metropolitan University, Tokyo 191-0065, Japan (e-mail: ntakesue@sd.tmu.ac.jp).

H. Fujimoto is with Nagoya Institute of Technology, Nagoya 466-8555, Japan (e-mail: fujimoto.hideo@nitech.ac.jp).

Digital Object Identifier 10.1109/TRO.2008.924947

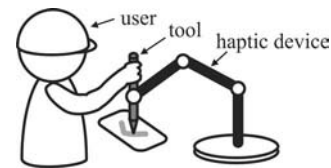


Fig. 1. Use of a haptic device for assisting manual tasks.

and direct-manipulation [10]–[13] tasks. The human-machine coordination using virtual fixtures will be useful especially in cases where the full automation is technically almost possible but is unacceptable due to reliability or economical reasons. Specifically, robot-assisted surgery [4], [12] and industrial assembly/disassembly processes [7] and [13] are potential fields of application. In addition, it has been suggested that they can be used for training of manipulation skills [5], [14].

This paper considers a class of virtual fixtures that act as hard walls but allow penetration according to the user’s decision. Allowing intended penetrations is important in cases where the computer’s decision that produces the virtual fixture is not fully reliable. Moreover, in some applications where safety is an utmost priority, it is preferred that the virtual fixtures do not store elastic potential energy even when it is penetrated. Producing such physical constraints is not a trivial matter. An elastic virtual wall stores elastic energy even if the force saturates at a particular level; the wall will pull the tool toward the wall surface irrespective of the moving direction of the tool as long as the tool is inside the wall. It can cause distraction to the user and unintended abrupt motion of the tool when the user relaxes his/her grasp on the tool. One example for an approach for producing nonenergy-storing virtual fixtures is the use of simulated viscosity, with which the velocity of the device is controlled to be roughly proportional to the user’s force [9], [11], [12]. In this approach, the force from the haptic device to the user always opposes the user’s motion, dissipating kinetic energy, and the motion in a nonpreferred direction is resisted by a large viscous resistance. A disadvantage of this approach may be that small and slow penetrations into the nonpreferred region are inevitable even if the user has no such intentions.

For producing penetratable, nonenergy-storing virtual fixtures, this paper presents an approach using simulated *plasticity*. Here the term “plasticity” is used to mean the characteristic of an object whereby it produces a permanent displacement under a force larger than a particular value (a yield force) but it does not produce any motion under a force smaller than the yield force. The Coulomb friction is an example for this characteristic; its

one-dimensional representation can be described as

$$f = -F\dot{q}/|\dot{q}| \quad (1)$$

where $f \in \mathbb{R}$ and $\dot{q} \in \mathbb{R}$ denote the resistance force and the velocity, respectively, and $F > 0$ denotes the yield force. The resistance force f always opposes the velocity \dot{q} , and thus, the force always dissipates the kinetic energy. The force f is discontinuous with respect to the velocity \dot{q} at $\dot{q} = 0$ and when $\dot{q} = 0$, the force f balances external forces to maintain zero velocity below the yield force F . Because of the discontinuous definition as in (1), the plasticity had been cumbersome to be implemented in discrete-time control systems. However, such difficulties have been removed by our recent achievement [15], which provides a mathematical framework for treating Coulomb-like friction in discrete time.

In the plasticity-based virtual fixture approach, the motion in a nonpreferred direction is resisted by a large yield force. One advantage of using plasticity instead of viscosity is supposed to be that the user can distinguish the direction in which the tool should not move *before* it actually starts to move. The tool is servo-controlled at a fixed position as long as the user's force is below the yield force, and thus, whether a direction is preferred or not can be recognized by whether the fixture yields or not in that direction. The initial idea of a plasticity-based virtual guide was presented in one of our previous papers [16], which proposed a "friction wall" for assisting precise path-tracing tasks. However, its aim of using plasticity was not discussed enough, and its algorithm was immature in that it can be used only with admittance-type haptic devices. Besides, it always produced remaining overshoots after crossing the path to be traced. This paper presents overall improvements of the "friction wall" algorithm with taking into account the nonenergy-storing property of plasticity.

We here emphasize that the property of being nonenergy storing is different from that of being passive. A real spring, in continuous time, is passive but energy storing. It has been known that elastic virtual walls presented through haptic devices can become nonpassive, generating extra energy, due to discretization of time and position measurements. Such an effect is not desirable, and extensive studies have been carried out to maintain the passivity of the discrete-time controllers of haptic devices [17]–[21]. This paper, however, does not present in-depth discussions on passivity. A part of our technique employs a virtual spring–damper element, but it is assumed that the stiffness and the viscosity coefficients for the virtual element are appropriately chosen not to violate passivity conditions.

The focus of this paper is placed on the technical challenge in realizing the concept of plasticity-based virtual fixtures with discrete-time controllers of haptic devices. Empirical human-factor studies on the efficacy of the presented technique are left for future work. Not always but in many cases, nonenergy-storing things can be considered intrinsically safer than energy-storing things. Among various nonenergy-storing dynamics, it is logical to assume that the plasticity is suited for the virtual fixture applications because it acts as a hard wall below a yield force, preventing unintended penetrations. The discontinuous nature of plasticity, however, gives rise to nontrivial technical problems

when it is used for producing virtual fixtures in discrete-time control systems. This paper aims to consolidate the solution for such technical problems in order to make this concept ready for trial applications and formal human-factor evaluation studies.

The rest of this paper is organized as follows. Section II revisits the mathematical framework for simulating plasticity in discrete time, which was proposed in [15], and presents the basic concept of plasticity-based virtual fixtures in one-dimensional space. Section III describes detailed control algorithms of plasticity-based virtual fixtures in multidimensional space. Section IV reports the results of implementation experiments obtained by using impedance-type and admittance-type haptic devices. Section V presents a modification to the presented algorithm for preventing unintended penetrations and demonstrates it through simple experiments. Section VI provides concluding remarks.

II. ONE-DIMENSIONAL PLASTICITY-BASED VIRTUAL FIXTURES

A. Mathematical Preliminaries

Some mathematical preliminaries are presented for the derivations in the upcoming sections. Let us define a generalized signum function as

$$\text{gsgn}(a, x, b) \begin{cases} = b, & \text{if } x > 0 \\ \in [a, b], & \text{if } x = 0 \\ = a, & \text{if } x < 0 \end{cases} \quad (2)$$

where $a \leq b$. Notice that it can take an arbitrary value between a and b when $x = 0$. Although gsgn is not a single-valued function, it can be used in equation-like and inequality-like expressions. The equation-like expression $y = \text{gsgn}(a, x, b)$ can be interpreted to be equivalent to the following logical expression:

$$(y = b \wedge x > 0) \vee (a \leq y \leq b \wedge x = 0) \vee (y = a \wedge x < 0). \quad (3)$$

Inequality-like expressions can be interpreted in the following manner:

$$y > \text{gsgn}(a, x, b) \iff (y > b \wedge x \geq 0) \vee (y > a \wedge x < 0) \quad (4)$$

$$y < \text{gsgn}(a, x, b) \iff (y < b \wedge x > 0) \vee (y < a \wedge x \leq 0). \quad (5)$$

Next, let us define a generalized saturation function as

$$\text{gsat}(a, x, b) = \begin{cases} b, & \text{if } x > b \\ x, & \text{if } x \in [a, b] \\ a, & \text{if } x < a \end{cases} \quad (6)$$

where $a \leq b$. This function returns x if $x \in [a, b]$ and returns the saturated value otherwise. Notice that the function gsat is a continuous, total, single-valued function.

Some implicit expressions involving gsgn can be equivalently rewritten as explicit expressions incorporating gsat . The following examples are important for the derivations throughout this

paper:

$$y = \text{gsgn}(a, x - y, b) \iff y = \text{gsat}(a, x, b) \quad (7)$$

$$y > \text{gsgn}(a, x - y, b) \iff y > \text{gsat}(a, x, b) \quad (8)$$

$$y < \text{gsgn}(a, x - y, b) \iff y < \text{gsat}(a, x, b). \quad (9)$$

The aforementioned examples are easily proven by converting them into logical expressions as in (3)–(5).

In the upcoming sections, the following equivalent expressions will be used

$$k(z - y) = \text{gsgn}(a, x - z, b) \iff z = y + \text{gsat}\left(\frac{a}{k}, x - y, \frac{b}{k}\right) \quad (10)$$

$$k(z - y) = \text{gsgn}(\text{gsgn}(a, -z, b), x - z, \text{gsgn}(c, -z, d)) \iff z = y + \text{gsat}\left(\frac{a}{k}, -y, \frac{b}{k}\right), \quad (11)$$

$$x - y, \text{gsat}\left(\frac{c}{k}, -y, \frac{d}{k}\right)$$

where $k > 0$ and $a \leq b \leq c \leq d$. The proofs for these rules directly follow the rules (7)–(9).

B. Simulated Plasticity

The plasticity is the dynamics with which the motion does not occur with an external force smaller than a yield force level and the resistance force is constant at any nonzero velocity. Consider an object with the position denoted by q . The relation between the force and the motion can be described as follows:

$$f = -\text{gsgn}(-F, \dot{q}, F) \quad (12)$$

where $F > 0$, notice that f can take an arbitrary value between $-F$ and F when $\dot{q} = 0$. Because the force f always opposes the velocity \dot{q} , the plasticity does not store energy and acts to dissipate the energy.

The use of (12) in haptic rendering is a cumbersome problem because the force f is indeterminate at $\dot{q} = 0$ and is discontinuous with respect to \dot{q} at $\dot{q} = 0$. For example, if the actuator force f is determined by using (12) with the measured velocity being used as \dot{q} , the haptic device will exhibit high-frequency oscillation due to repeated zero-velocity crossings. As is detailed in the literature survey in [15], many mathematical models of friction have been proposed, but they suffer from either of chattering, unbounded drift, or difficulties in extension to multidimensional cases. The paper [15] has presented a unified, mathematically consistent treatment of the discontinuity such as (12) to be used in a broad class of haptic rendering systems.

Here, the techniques presented in [15] are explained in slightly different notational conventions. There are two types of haptic rendering schemes: the impedance type and the admittance type. In the impedance-type scheme, the position p of the tool (haptic device) is measured, the reaction force f from the virtual world is calculated, and the force f is produced by the actuators. In the admittance-type scheme, the force h applied from the user is measured by force sensors, the position q of a virtual object in

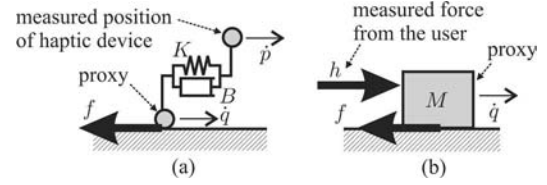


Fig. 2. Physical models on which the friction (plasticity) models in [15] are based. (a) Impedance type. (b) Admittance type.

the virtual world is updated, and the tool position is controlled to follow the position q by using as stiff a position controller as possible. If the haptic device is backdrivable enough, the impedance type can be chosen. Otherwise, the admittance type should be chosen with a force sensor being mounted on the device.

For simulating the plasticity in impedance-type haptic rendering, we must consider a massless virtual object (a proxy) in the software, as illustrated in Fig. 2(a). It is connected to the tool through a virtual spring–damper element (a virtual coupling). The use of such intermediate virtual elements is a well-established technique in the field of haptic rendering [18], [22]–[24]. One of our contributions in the previous paper [15] was a mathematically consistent formulation of the combination of a damped virtual coupling and a proxy for simulating plasticity. Let q denote the position of the proxy. The proxy accepts the plastic force (12) and the spring–damper force, which is described as

$$f = K(q - p) + B(\dot{q} - \dot{p}) \quad (13)$$

where K and B are the stiffness and viscosity coefficients of the virtual coupling. The force produced by the virtual coupling f of (13) always balances the plastic force f of (12). Thus, both of them are denoted by f . In other words, the force f satisfies both (12) and (13). In general, the parameters K and B should be set as high as possible because a lower stiffness will increase the influence of the fluctuation of the user's force. The upper limit for K and B can be found by addressing the previous theoretical studies on stability and passivity [8], [17]–[21]. This paper, however, simply assumes that K and B are appropriately chosen not to affect stability and passivity, leaving the optimal choice of the values outside its scope.

In the admittance type, on the other hand, we must consider a virtual object having a nonzero mass M . We also call this object as a proxy hereafter. The input force h and the force f of (12) act to the proxy, as shown in Fig. 2(b). Thus, the equation of motion of the proxy is written as

$$f = M\ddot{q} - h. \quad (14)$$

In general, the parameter M should be set as low as permitted by the bandwidth of the position control loop (including the haptic device) because a higher inertia is usually undesirable for accurate manual tasks. The optimal choice of M is also left outside the scope of this paper.

Although the plasticity itself does not store energy, the virtual coupling in (13) and the virtual mass in (14) store energy. We do not consider it a serious problem because these virtual

elements can be considered as media between the simulated nonenergy-storing dynamics (12) and the haptic device. Since a haptic device itself possesses compliance and mass, which store some elastic and kinetic energy, the virtual coupling and mass can be said to have some effects of enhancing the energy-storing property of the haptic device. They, however, do not defeat the significance of the simulated plasticity because, if the combination of the device and the virtual coupling/mass is sufficiently stiff and lightweight, the user's experience through the haptic device is mostly determined by the design of the simulated plasticity. Another remark here is that, in the impedance-type implementation, the elastic energy stored by the virtual coupling is bounded by $F^2/(2K)$, which indicates that the amount of the elastic energy that can be stored is reduced by choosing a higher value for K .

Based on the backward Euler scheme, (13) and (14) are, respectively, rewritten as follows:

$$f(i) = K(q(i) - p(i)) + \frac{B(q(i) - q(i-1) - p(i) + p(i-1)))}{T} \quad (15)$$

$$f(i) = \frac{M(q(i) - 2q(i-1) + q(i-2))}{T^2} - h(i). \quad (16)$$

Here, T is the time step size and the arguments in the parentheses, such as i and $i-1$, are integers indicating discrete-time indices. Both (15) and (16) can be rewritten as

$$f(i) = \kappa(q(i) - p^*(i)) \quad (17)$$

where

$$\kappa = K + \frac{B}{T} \quad (18)$$

$$p^*(i) = \frac{p(i) + B(q(i-1) - p(i-1))}{(KT + B)} \quad (19)$$

in the case of (15), the impedance type, and

$$\kappa = \frac{M}{T^2} \quad (20)$$

$$p^*(i) = \frac{2q(i-1) - q(i-2) + T^2 h(i)}{M} \quad (21)$$

in the case of (16), the admittance type. The use of a common form (17) for both impedance- and admittance-type haptic rendering is detailed in [24]. Note that $p^*(i)$ can be treated as a known variable because it only depends on past values [$p(i-1)$, $q(i-1)$, and $q(i-2)$] and current input values [$p(i)$ and $h(i)$]. It can be interpreted as the proxy position that could have been achieved if $f(i) = 0$, i.e., if no plastic force $f(i)$ acted. We hereafter refer to $p^*(i)$ as the *input position*.

Also based on the backward Euler scheme, (12) can be rewritten as

$$f(i) = \text{gsgn}(-F, q(i-1) - q(i), F). \quad (22)$$

Substituting (17) into (22) yields

$$\kappa(q(i) - p^*(i)) = \text{gsgn}(-F, q(i-1) - q(i), F). \quad (23)$$

The current proxy position $q(i)$ has to be determined so that it satisfies (23). The application of rule (10) shows that the solution

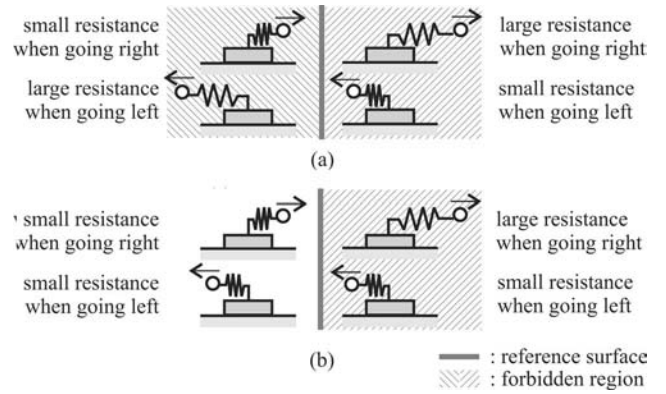


Fig. 3. Basic concept of plasticity-based virtual fixtures. (a) Bilateral virtual fixture. (b) Unilateral virtual fixture.

for (23) is

$$q(i) = p^*(i) + \text{gsat}\left(\frac{-F}{\kappa}, q(i-1) - p^*(i), \frac{F}{\kappa}\right). \quad (24)$$

In conclusion, the computational procedure to realize plastic responses in impedance-type haptic rendering is given as follows:

$$p^*(i) = \frac{p(i) + B(q(i-1) - p(i-1))}{(KT + B)} \quad (25)$$

$$q(i) = p^*(i) + \text{gsat}\left(\frac{-F}{\kappa}, q(i-1) - p^*(i), \frac{F}{\kappa}\right) \quad (26)$$

$$f(i) = \kappa(q(i) - p^*(i)) \quad (27)$$

where $\kappa = K + B/T$. In the admittance type, on the other hand, it is given as

$$p^*(i) = \frac{2q(i-1) - q(i-2) + T^2 h(i)}{M} \quad (28)$$

$$q(i) = p^*(i) + \text{gsat}\left(\frac{-F}{\kappa}, q(i-1) - p^*(i), \frac{F}{\kappa}\right) \quad (29)$$

where $\kappa = M/T^2$.

Equation (24) can also be expressed as

$$q(i) = \underset{q \in \mathcal{A}(p^*(i))}{\text{argmin}} |q - q(i-1)| \quad (30)$$

where

$$\mathcal{A}(p^*(i)) = \left\{ q \in \mathbb{R} \mid \frac{-F}{\kappa} \leq q - p^*(i) \leq \frac{F}{\kappa} \right\}. \quad (31)$$

Here, $\mathcal{A}(p^*(i))$ can be viewed as the set of the admissible values for $q(i)$, and (30) shows that the proxy position $q(i)$ is determined so that it minimizes the distance from $q(i-1)$.

C. Plasticity-Based Virtual Fixtures

The use of the simulated plasticity for virtual fixtures is now presented. Its basic concept is illustrated in Fig. 3. We here consider two types of virtual fixtures: bilateral and unilateral. A bilateral one acts to prevent the tool from departing from a reference surface (or curve). A unilateral one acts to prevent the tool from entering a nonpreferred region, which should not be entered. We also refer to the boundary of the unilateral virtual

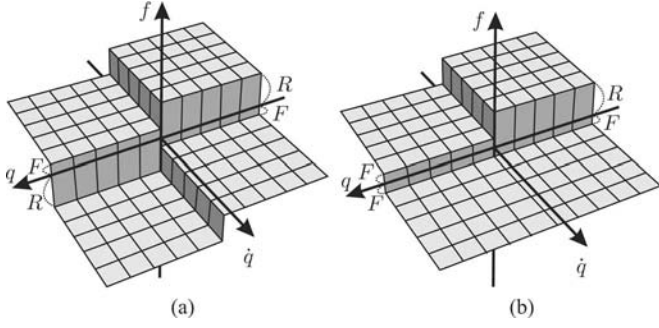


Fig. 4. Relations between f , q , and \dot{q} with one-dimensional bilateral (a) and unilateral (b) virtual fixtures.

fixture as a reference surface. A plasticity-based virtual fixture generates a large resistance force when the user is moving deeper into the nonpreferred region. Otherwise, it generates a small resistance force for helping stable task execution by canceling unintended tremors or disturbances, as demonstrated in [25]. The force always opposes the velocity (precisely, the proxy's velocity), and thus, these virtual fixtures always dissipate the kinetic energy.

Let $q = 0$ be the reference surface in one-dimensional space. Then, the force f from a bilateral virtual fixture to the proxy can be written as

$$f = -\text{gsgn}(\text{gsgn}(-R, q, -F), \dot{q}, \text{gsgn}(F, q, R)) \quad (32)$$

where $R \gg F > 0$. A unilateral virtual fixture, on the other hand, can be described as

$$f = -\text{gsgn}(\text{gsgn}(-R, q, -F), \dot{q}, F) \quad (33)$$

where $\{q \in \mathbb{R} \mid q < 0\}$ is assumed to be the nonpreferred region. The relations (32) and (33) are illustrated in Fig. 4(a) and (b), respectively. Notice that f can take intermediate values other than $\pm R$ or $\pm F$ when $q = 0$ or $\dot{q} = 0$.

The plastic characteristics of (32) and (33) can be implemented in discrete-time systems in the same manner in Section II-B. Let us replace f by $\kappa(q(i) - p^*(i))$ and \dot{q} by $(q(i) - q(i-1))/T$. Then, (32) becomes

$$\begin{aligned} \kappa(q(i) - p^*(i)) = & -\text{gsgn}(\text{gsgn}(-R, q(i), -F), \\ & q(i) - q(i-1), \text{gsgn}(F, q(i), R)) \end{aligned} \quad (34)$$

and (33) becomes

$$\begin{aligned} \kappa(q(i) - p^*(i)) = & -\text{gsgn}(\text{gsgn}(-R, q(i), -F), \\ & q(i) - q(i-1), F). \end{aligned} \quad (35)$$

The solution for (34) is obtained by the application of the rule (11), which yields

$$q(i) = p^*(i) + \text{gsat}(-a_1(i), q(i-1) - p^*(i), a_2(i)) \quad (36)$$

where

$$a_1(i) = \text{gsat}\left(\frac{F}{\kappa}, p^*(i), \frac{R}{\kappa}\right) \quad (37)$$

$$a_2(i) = \text{gsat}\left(\frac{F}{\kappa}, -p^*(i), \frac{R}{\kappa}\right). \quad (38)$$

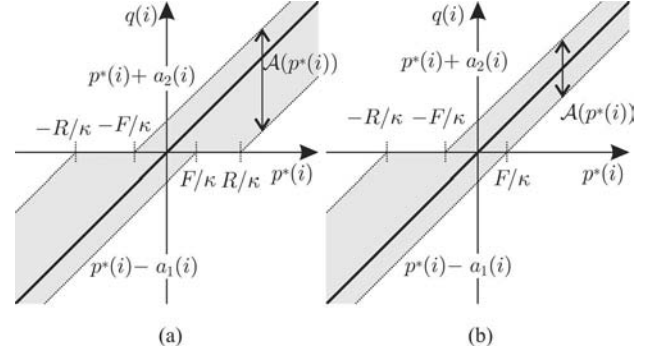


Fig. 5. Set $\mathcal{A}(p^*(i))$ of possible new proxy positions $q(i)$ in one-dimensional bilateral (a) and unilateral (b) virtual fixtures.

The solution for (35) is obtained in the same manner; it is the same as (36) but where $a_1(i)$ and $a_2(i)$ have the following different definitions:

$$a_1(i) = \frac{F}{\kappa} \quad (39)$$

$$a_2(i) = \text{gsat}\left(\frac{F}{\kappa}, -p^*(i), \frac{R}{\kappa}\right). \quad (40)$$

In both cases, the set $\mathcal{A}(p^*(i))$, which is the set of admissible proxy positions $q(i)$, can be represented as follows:

$$\mathcal{A}(p^*(i)) = \{q \in \mathbb{R} \mid -a_1(i) \leq q - p^*(i) \leq a_2(i)\} \quad (41)$$

which is shown in Fig. 5. Equation (36) substitutes (26) and (29) in the impedance-type and admittance-type implementation, respectively.

We here emphasize that the aforementioned technique is based only on simple concepts of the plasticity-based virtual fixtures, which is represented in Figs. 3–5 and (32) and (33), and standard intermediate virtual elements (13) and (14). The derivation can be done with keeping a few formulas in Section II-A in mind. There might exist different algorithms that behave similarly to the described algorithm but it is likely that they would require elaborate (sometimes *ad hoc*) logic programming to avoid subtle but nonnegligible problems that will surface in the implementation. For example, one imaginable idea is to consider an elastic wall that moves away from the reference surface when the applied force exceeds a predetermined level but moves back to the reference surface when the user's motion is pointing toward the surface. Such an approach will encounter a chattering problem due to the noise in the measurements of the direction of the user's motion, which is inherently the same problem as the one discussed in Section II-B and the previous paper [15]. Moreover, such an algorithm will require overall modification to be adapted to admittance-type implementation.

III. MULTIDIMENSIONAL VIRTUAL FIXTURES

A. Geometric Representation of Anisotropic Plasticity

This section extends the idea of plasticity-based virtual fixtures into multidimensional space. Sections II-B and II-C have shown that the plasticity in one-dimensional space is represented by a set of admissible proxy positions $\mathcal{A}(p^*(i))$, of which a larger

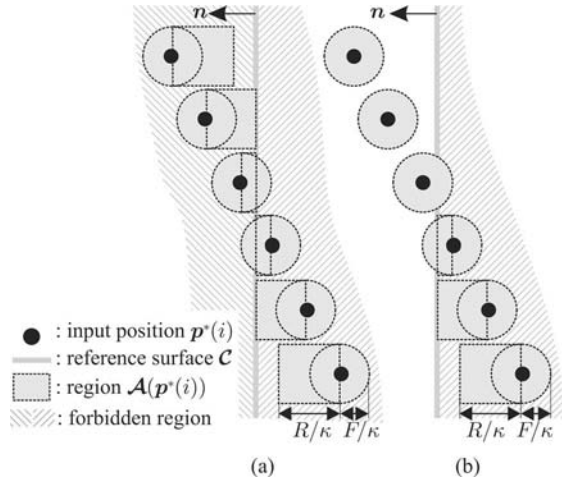


Fig. 6. Geometric representations of the set $\mathcal{A}(\mathbf{p}^*(i))$. (a) For a bilateral virtual fixture. (b) For a unilateral virtual fixture.

size indicates a larger yield force. This section extends this idea to represent anisotropic plasticity in n -dimensional space. Hereafter, boldface symbols denote vectors correspondent to scalars in Section II. The new proxy position $\mathbf{q}(i)$ is determined to be the position nearest to the previous proxy position $\mathbf{q}(i-1)$ within the set $\mathcal{A}(\mathbf{p}^*(i))$, which depends on the input position $\mathbf{p}^*(i)$. This rule is concisely described as

$$\mathbf{q}(i) = \underset{\mathbf{q} \in \mathcal{A}(\mathbf{p}^*(i))}{\operatorname{argmin}} \|\mathbf{q} - \mathbf{q}(i-1)\|. \quad (42)$$

This section discusses how the set $\mathcal{A}(\mathbf{p}^*(i))$ should be defined to produce plasticity-based virtual fixtures and how the new proxy position $\mathbf{q}(i)$ should be chosen to satisfy (42).

We treat the case in which the reference surface \mathcal{C} is defined as an $(n-1)$ -dimensional subspace in n -dimensional space: \mathcal{C} is a flat plane in three-dimensional space or is a straight line in two-dimensional space. The tool should be constrained on \mathcal{C} if it is bilateral but \mathcal{C} is the boundary of a nonpreferred region if it is unilateral. For producing such virtual fixtures, we propose to use the anisotropic plasticity that is geometrically represented in Fig. 6. It is mathematically described as

$$\mathcal{A}(\mathbf{p}^*(i)) = \mathcal{A}_F(\mathbf{p}^*(i)) \cup \mathcal{A}_R(\mathbf{p}^*(i)) \quad (43)$$

where

$$\mathcal{A}_F(\mathbf{p}^*(i)) = \left\{ \mathbf{q} \in \mathbb{R}^n \mid \|\mathbf{q} - \mathbf{p}^*(i)\| \leq \frac{F}{\kappa} \right\} \quad (44)$$

$$\mathcal{A}_R(\mathbf{p}^*(i)) = \left\{ \mathbf{q} \in \mathbb{R}^n \mid \|\mathbf{N}^T(\mathbf{q} - \mathbf{p}^*(i))\| \leq \frac{F}{\kappa} \right. \\ \left. \wedge -a_1(i) \leq \mathbf{n}^T(\mathbf{q} - \mathbf{p}^*(i)) \leq a_2(i) \right\} \quad (45)$$

and

$$a_1(i) = \begin{cases} \operatorname{gsat} \left(0, \mathbf{n}^T(\mathbf{p}^*(i) - \mathbf{r}_C(i)), \frac{R}{\kappa} \right), & \text{if bi} \\ 0, & \text{if uni} \end{cases} \quad (46)$$

$$a_2(i) = \operatorname{gsat} \left(0, -\mathbf{n}^T(\mathbf{p}^*(i) - \mathbf{r}_C(i)), \frac{R}{\kappa} \right). \quad (47)$$

Here, \mathbf{n} is the unit normal vector of \mathcal{C} projecting outward from the nonpreferred region in the unilateral case. (In the bilateral case, the direction does not matter.) The matrix \mathbf{N} is a column-full rank matrix that satisfies

$$\mathbf{N} \in \mathbb{R}^{n \times (n-1)}, \quad \mathbf{N}^T \mathbf{n} = \mathbf{o}, \quad \mathbf{N} \mathbf{N}^T + \mathbf{n} \mathbf{n}^T = \mathbf{I}. \quad (48)$$

It follows that

$$\|\mathbf{N}^T \mathbf{x}\| = \sqrt{\|\mathbf{x}\|^2 - (\mathbf{n}^T \mathbf{x})^2} \quad \forall \mathbf{x} \in \mathbb{R}^n \quad (49)$$

and, as a special case, $\|\mathbf{N}^T \mathbf{x}\| = \|\mathbf{n} \times \mathbf{x}\|$ in three-dimensional space ($n=3$). The set $\mathcal{A}_F(\mathbf{p}^*(i))$ represents the circular (or spherical) region centering $\mathbf{p}^*(i)$. The set $\mathcal{A}_R(\mathbf{p}^*(i))$ is a rectangular (or cylindrical) region with a width (or diameter) $2F/\kappa$ and a length no larger than R/κ . The circular region $\mathcal{A}_F(\mathbf{p}^*(i))$ is for producing isotropic plastic response outside the nonpreferred region for helping stable task executions by canceling unintended tremors or disturbances. The rectangular region $\mathcal{A}_R(\mathbf{p}^*(i))$ is for producing a large yield force R to prevent the tool from entering the nonpreferred region.

Under the anisotropic plasticity characterized by $\mathcal{A}(\mathbf{p}^*(i))$ in (43), the new proxy position $\mathbf{q}(i)$ can be determined as

$$\mathbf{q}(i) = \underset{\mathbf{q} \in \mathcal{A}_F(\mathbf{p}^*(i))}{\operatorname{argmin}} \|\mathbf{q} - \mathbf{q}(i-1)\| \quad (50)$$

$$\mathbf{q}_F(i) = \underset{\mathbf{q} \in \mathcal{A}_F(\mathbf{p}^*(i))}{\operatorname{argmin}} \|\mathbf{q} - \mathbf{q}(i-1)\| \quad (51)$$

$$\text{IF } \|\mathbf{q}_F(i) - \mathbf{q}(i-1)\| \leq \|\mathbf{q}(i) - \mathbf{q}(i-1)\| \text{ THEN} \quad (52)$$

$$\mathbf{q}(i) := \mathbf{q}_F(i) \quad (53)$$

$$\text{ENDIF} \quad (54)$$

where $:=$ means overwriting. Considering the simple spherical geometry of the set $\mathcal{A}_F(\mathbf{p}^*(i))$, $\mathbf{q}_F(i)$ in (51) can be easily rewritten as

$$\mathbf{q}_F(i) = \mathbf{p}^*(i) + \operatorname{sat} \left(\mathbf{q}(i-1) - \mathbf{p}^*(i), \frac{F}{\kappa} \right) \quad (55)$$

where

$$\operatorname{sat}(\mathbf{x}, a) = \frac{\mathbf{x}}{\max(1, \|\mathbf{x}\|/a)} \\ = \begin{cases} \mathbf{x} & \text{if } \|\mathbf{x}\| \leq a \\ a \frac{\mathbf{x}}{\|\mathbf{x}\|} & \text{if } \|\mathbf{x}\| > a. \end{cases} \quad (56)$$

The problem still remaining is to solve (50), which relates to the rectangular region $\mathcal{A}_R(\mathbf{p}^*(i))$. We can derive $\mathbf{q}(i)$ by separating it into the components normal to and tangential to \mathcal{C} . The component of a vector \mathbf{x} tangential to \mathcal{C} is described as $\mathbf{N}^T \mathbf{x} (\in \mathbb{R}^{n-1})$. Because the projection of $\mathcal{A}(\mathbf{p}^*(i))$ onto \mathcal{C} is a simple circle with a radius F/κ centering at $\mathbf{N}^T \mathbf{p}^*(i)$, the tangential component of $\mathbf{q}(i)$ can be obtained as follows:

$$\mathbf{N}^T \mathbf{q}(i) = \mathbf{N}^T \mathbf{p}^*(i) + \operatorname{sat} \left(\mathbf{N}^T(\mathbf{q}(i-1) - \mathbf{p}^*(i)), \frac{F}{\kappa} \right). \quad (57)$$

Meanwhile, the component of a vector \mathbf{x} normal to \mathcal{C} is written as $\mathbf{n}^T \mathbf{x} (\in \mathbb{R})$. In the normal direction, the length of the

ELSE (80)

IsOn(i) = IsOn($i - 1$) (81)

END IF (82)

IF IsOn(i) = TRUE THEN (83)

$q(i) := \operatorname{argmin}_{r \in \mathcal{C}} \|r - q(i)\|$ (84)

END IF. (85)

The new proxy position $q(i)$ is snapped onto \mathcal{C} by (84) if the flag IsOn(i) is TRUE. It is true if $\mathcal{A}_R(p^*(i))$ is in contact with $\hat{\mathcal{C}}(i)$, the previous proxy position $q(i - 1)$ and the input position $p^*(i)$ are on different sides of $\hat{\mathcal{C}}(i)$, and the interim new proxy position $q(i)$ is outside of $\mathcal{A}_F(p^*(i))$. Note that this algorithm is an approximation that sacrifices the guarantee of $q(i) \in \mathcal{A}_F(p^*(i))$ in order to guarantee $q(i) \in \mathcal{C}$ when IsOn(i) is TRUE because $q(i) \in \mathcal{C}$ is important for the accuracy in tracing the reference surface \mathcal{C} .

IV. IMPLEMENTATION

The proposed algorithm (75)–(85) was tested with two distinctly different haptic devices. One was an impedance-type haptic device, which was sufficiently backdrivable. The other was an admittance-type haptic device, which had heavy joint friction and large inertia but was equipped with a force/torque sensor. Different types of implementation schemes should be adopted for these two devices, but the algorithm (75)–(85) can be used in both cases.

The purpose of this section is to demonstrate the algorithm's capability of realizing the concept of plasticity-based virtual fixtures on both of impedance-type and admittance-type haptic devices. This section, therefore, does not present empirical comparisons between plasticity-based virtual fixtures to conventional virtual fixtures. Another reason to avoid such comparisons is that conventional approaches generally require some modifications to be used with both of impedance-type and admittance-type devices. Thus, qualitative comparisons between new and conventional algorithms in a specific implementation would make little sense. The practical benefit of plasticity-based virtual fixtures over conventional virtual fixtures would be clarified through formal human-factor studies involving many human participants under some specific manual tasks. Such studies are left outside the scope of this paper.

The comparison between the impedance-type and the admittance-type implementation is not presented either. This is because the choice of the control scheme depends on the type of the device, and the comparison between the two types with a common haptic device requires a device with both of a force sensor and sufficient backdrivability, which would be uneconomical for practical use.

A. Impedance-Type Implementation

The proposed algorithm was implemented in a SensAble PHANTOM Omni device, which was capable of 3 DOF actuation and 6 DOF measurements. The measured position $p(i)$

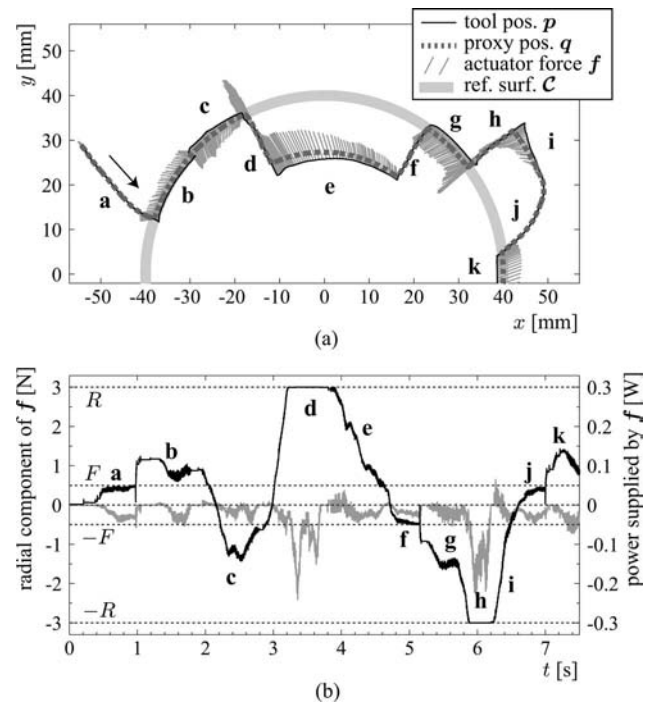


Fig. 8. Experimental results with impedance-type implementation of a bilateral virtual fixture. The radial component of f means the component of the force f in the direction away from the axis of the cylindrical reference surface \mathcal{C} to the tool position p . The power is calculated by taking the inner product of the tool velocity vector (after a five-point moving average smoothing) and the force vector f . (a) Tool and proxy trajectories and actuator forces. (b) Time t versus force (black) and power (gray).

of the tool (stylus) of the device was converted into the input position $p^*(i)$ by (25), and the proxy position $q(i)$ was determined through the procedure (75)–(85). The actuator force $f(i)$ was determined by (27). The sampling interval was set to be $T = 0.001$ s. The reference surface \mathcal{C} was chosen as a cylindrical surface with a radius of 40 mm whose axis coincides with the z -axis. The parameters were chosen as $K = 1$ N/mm, $B = 0.0015$ Ns/mm, $F = 0.5$ N, and $R = 3$ N. These values of K and B were chosen as high as possible without affecting the stability of the device. The value of F was chosen to produce a moderate frictional resistance for stable manual motion and R was chosen to produce a distinct resistance. The tool was manually operated by an experimenter.

Fig. 8 shows the results obtained when \mathcal{C} was set to be a bilateral virtual fixture. It is shown that, when the tool was approaching to \mathcal{C} (a, f, and j), the force f was small, being at the level no larger than F . In contrast, when the tool was moving away from \mathcal{C} (d and h), the force was large, being at the level of R . When the experimenter was on \mathcal{C} , the proxy was constrained on \mathcal{C} both when the tool was pushed inward (b and k) and when pushed outward (c and g) with the force smaller than R . The experimenter was able to deviate from \mathcal{C} by applying a force larger than the yield force R (d and h). When the experimenter was not on \mathcal{C} , the motion tended to be parallel to \mathcal{C} when the tool was being pushed away from \mathcal{C} with a force smaller than R (e and i) because any motions away from \mathcal{C} were resisted by the larger yield force R .

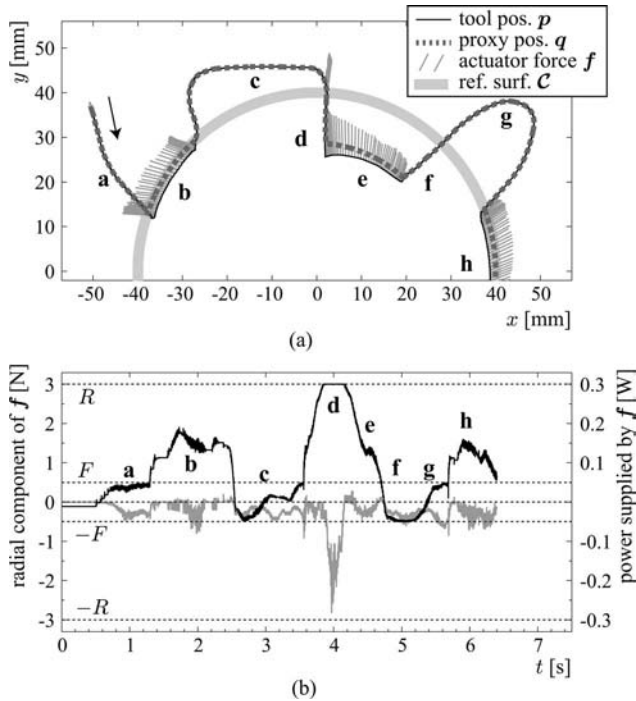


Fig. 9. Experimental results with impedance-type implementation of a unilateral virtual fixture. The definitions of the force component and the power are the same as those in Fig. 8. (a) Tool and proxy trajectories and actuator forces. (b) Time t versus force (black) and power (gray).

The gray plot in Fig. 8(b) shows that the power delivered by the actuator to the tool was almost always negative, which means that the force almost always opposed to the experimenter's motion to dissipate the kinetic energy. The power took small positive values only during short transient periods when the experimenter started to relax his force (beginnings of e and i). This is attributed to the small elastic energy stored in the virtual coupling connecting the tool and the proxy, which can be reduced by choosing a higher K value (as discussed in Section II-B) as far as permitted by the stability of the device.

Fig. 9 shows the results obtained when \mathcal{C} was set to be a unilateral virtual fixture whose nonpreferred region was inside the cylinder. It is shown that, when the tool was moving deeper below the surface \mathcal{C} (d), the radial component of the force f was large at the level of R . In contrast, when it was outside \mathcal{C} (a, c, and g) and when it was below the surface but moving shallower (f), the force was no larger than F . The proxy was constrained on \mathcal{C} (b and h) when the tool was pushed onto the surface \mathcal{C} with the force being smaller than R but it can be penetrated by applying the force larger than R (d). As was the case with the bilateral fixture in Fig. 8, the motion tended to be parallel to \mathcal{C} when the tool was being pushed inward with a force smaller than R (e). The power delivered from the actuators to the device was almost always negative except some short transient periods.

In both cases, the actuator force f was able to take intermediate values smaller than F or R in the static friction state (i.e., when the tool is stationary). Thus, the presented algorithm did not cause chattering due to zero-velocity crossings. This property is inherited from our basic technique of simulating

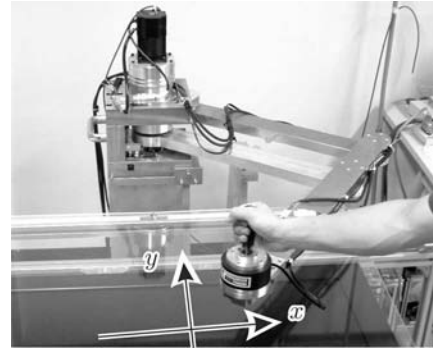


Fig. 10. Parallel-link manipulator used as an admittance-type haptic device.

plasticity, which is overviewed in Section II-B and detailed in our previous paper [15].

B. Admittance-Type Implementation

The proposed algorithm was also implemented in an admittance-type haptic device, which is shown in Fig. 10. It was a 2-DOF parallel link manipulator actuated by two ac servo motors with harmonic drive gears. The joint friction was approximately 10 N-m for both joints. The joint angles were measured by optical encoders attached to the servo motors. A six-axis force sensor (Nitta IFS) was mounted on the end-effector. The system was controlled by using a personal computer running ART-Linux. A handle grip (the tool) attached to the force sensor was grasped and moved by an experimenter.

The measured force $h(i)$ applied from the experimenter's hand was used to calculate the input position $p^*(i)$ by (28), and the proxy position $q(i)$ was determined through the procedure (75)–(85). The position of the tool was controlled to track the proxy position $q(i)$ by using stiff PID control¹ in the Cartesian space. The sampling interval was set to be $T = 0.001$ s. The reference surface \mathcal{C} was chosen as a circle with a radius of 120 mm whose center coincides with the origin. The parameters were chosen as $M = 2$ kg, $F = 3$ N, and $R = 20$ N. This value of M was chosen as small as possible without affecting the stability of the admittance control with this device. The value of F was chosen to produce a moderate frictional resistance for stable manual motion and R was chosen to produce a distinct resistance.

The results are shown in Figs. 11 and 12. The force vectors in these figures are $-h$, which is the opposite of the force sensor measurement and is the force applied from the robot's end-effector to the experimenter's hand. Note that the force vectors in these figures are the (reversed) measured forces while those in Figs. 8 and 9 were the actuator forces. Figs. 11 and 12 show features similar to the data in Figs. 8 and 9, exhibiting the validity of the presented algorithm. The experimenter was able to deviate from \mathcal{C} by applying a force larger than the yield force R (d and h in Fig. 11; d in Fig. 12) but he was able to trace \mathcal{C}

¹To be more exact, we employed the proxy-based sliding mode control scheme [26] for safety reasons. It is equivalent to the ordinary PID control scheme as long as the actuator torques were below saturation, which was the case in this experiment.

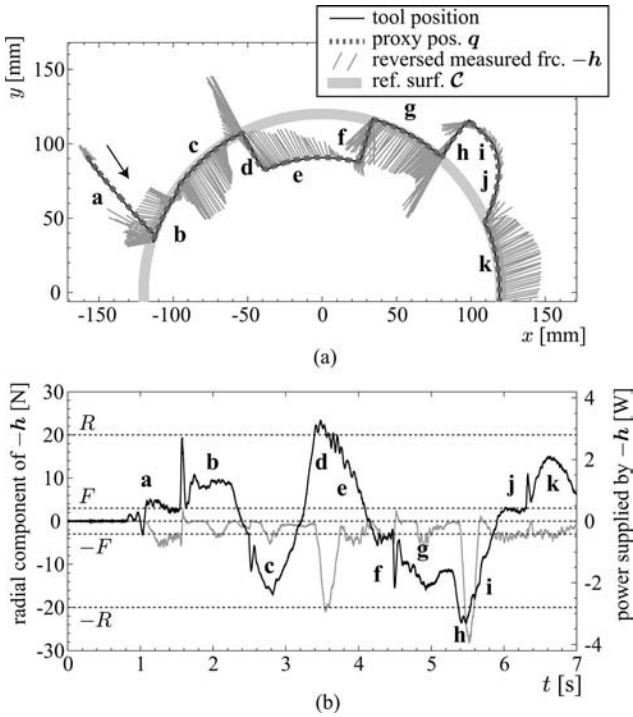


Fig. 11. Experimental results with admittance-type implementation of a bilateral virtual fixture. The radial component of $-\mathbf{h}$ means the component of the force $-\mathbf{h}$ in the direction away from the center of the circular reference surface \mathcal{C} to the tool position. The power is calculated by taking the inner product of the tool velocity vector (after a five-point moving average smoothing) and the force vector $-\mathbf{h}$. (a) Tool and proxy trajectories and measured forces. (b) Time t versus force (black) and power (gray).

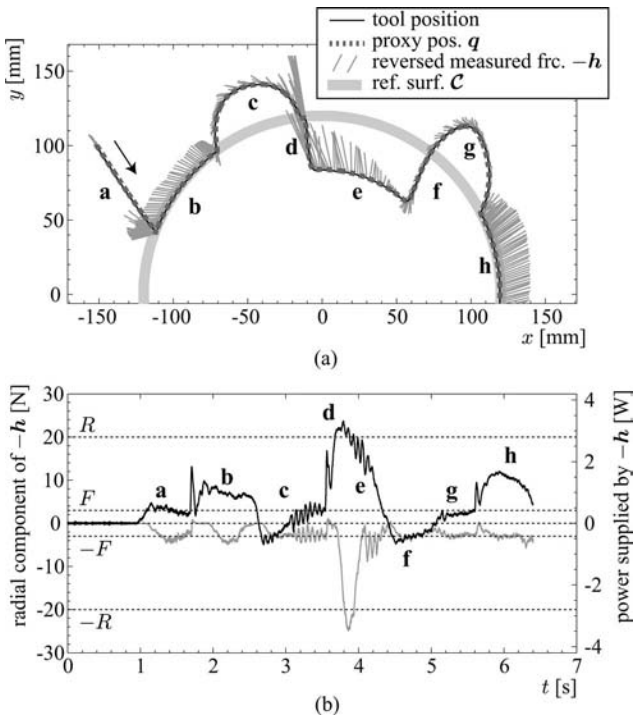


Fig. 12. Experimental results with admittance-type implementation of a unilateral virtual fixture. The definitions of the force component and the power are the same as those in Fig. 11. (a) Tool and proxy trajectories and measured forces. (b) Time t versus force (black) and power (gray).

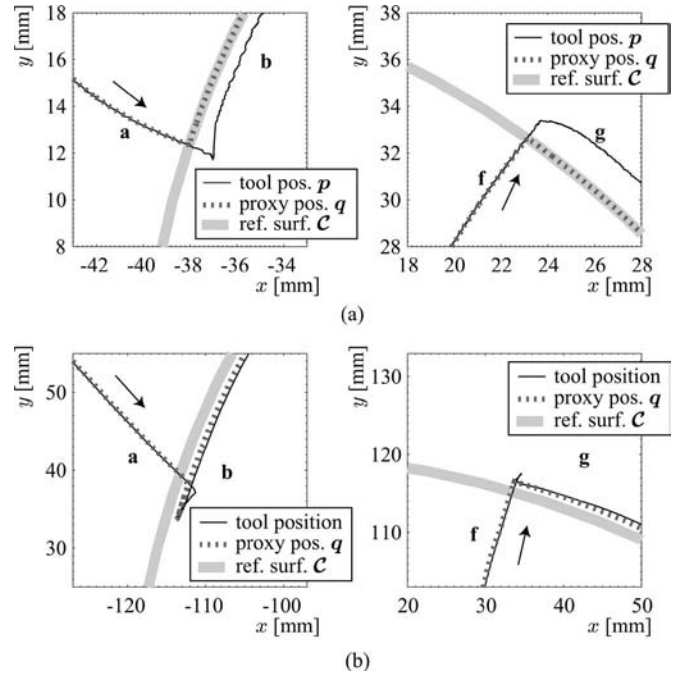


Fig. 13. Magnified views of (a) Fig. 8 (impedance type) and (b) Fig. 11 (admittance type).

with a force smaller than R (b, c, g, and k in Fig. 11; b and h in Fig. 12).

The gray plots in Figs. 11(b) and 12(b) show that the power delivered from the tool to the experimenter's hand was almost always negative, dissipating kinetic energy. It took very small positive values only when the experimenter's hand is abruptly decelerated due to collisions to the forbidden regions (the beginnings of b, g, and k in Fig. 11; the beginnings of b, d, and h in Fig. 12). This is attributed to the small kinetic energy stored in the haptic device and the virtual mass, which can be reduced by choosing a lower M value as far as permitted by the stability of the admittance control.

Although the results shown in Figs. 11 and 12 appear to be fair, it was observed that the proxy penetrated the reference surface \mathcal{C} for a few millimeters after impacting the surface. Such penetrations were not observed in the impedance-type implementation. Fig. 13(a) and (b) is a magnified view of Figs. 8(a) and 11(a), respectively, with the force vectors being removed. They clearly show that, in the admittance-type implementation [Fig. 13(b)], the proxy penetrated \mathcal{C} after the collisions,² but in the impedance-type implementation [Fig. 13(a)], the proxy was captured on \mathcal{C} . This difference cannot be neglected because the penetration of the proxy is not recovered unless the user pushes back the tool toward \mathcal{C} . The unintended penetrations in the admittance-type implementation were observed especially when the colliding velocity was not slow enough and when R was small. The cause of the penetration is that the momentum

²In Fig. 13(b, left), there is a small motion toward bottom left after the collision with \mathcal{C} . We place no significance for this because it is presumably due only to the fluctuation of the experimenter's hand. The experimenter intended to slide the tool in the top right direction along \mathcal{C} after keeping the tool stationary on \mathcal{C} for a moment.

preserved by the proxy with a nonzero mass M can fail to become zero instantly with a resistance force of a finite magnitude. Next section discusses this phenomenon in detail.

V. MODIFICATION TO PREVENT POSTIMPACT PENETRATIONS

This section presents a modification to the virtual fixture algorithm to prevent the postimpact penetrations observed in the implementation experiments in Section IV-B.

It is important to recognize that a postimpact penetration is a direct consequence of the mathematical representations of the ideal plasticity presented in Section II. Specifically, the expressions (32) and (33) cannot produce a force f larger than the yield force R although a mass M moving at a velocity v can stop within a time interval T only by applying the force Mv/T , which can exceed R when T is small. In the continuous-time system where $T = 0$, it is impossible for a nonzero mass to stop exactly on the reference surface \mathcal{C} .

Postimpact penetrations did not occur in the impedance-type implementation demonstrated in Fig. 13(b). This is because the impedance-type implementation was much *softer* than the admittance-type implementation in the sense that the value of κ , which is the equivalent spring coefficient, was $\kappa = K + B/T = 2.5$ N/mm in the impedance type and $\kappa = M/T^2 = 2000$ N/mm in the admittance type. The longitudinal length of the rectangular part of the set \mathcal{A} was $R/\kappa = 1.2$ mm in the impedance type, which was much longer than $R/\kappa = 0.01$ mm in the admittance type. If the proxy velocity is lower than $R/(\kappa T)$ when it crosses the reference surface \mathcal{C} , the proxy is captured by \mathcal{C} , but otherwise it can skip \mathcal{C} , resulting in a postimpact penetration.

Although a postimpact penetration is a correct consequence from a mathematical point of view, it is undesirable from a practical point of view. One approach for removing a postimpact penetration is to compulsorily keep the proxy on the reference surface \mathcal{C} for several time steps after an impact. Based on this idea, a possible modification to the algorithm (75)–(85) can be obtained as follows:

RUN (64) TO (74) (86)

IF $\mathbf{n}(i)^T \mathbf{k}(i) \notin \left\{ \begin{array}{l} [-R/\kappa, R/\kappa] \text{ if bi.} \\ [-R/\kappa, 0] \text{ if uni.} \end{array} \right\}$ THEN (87)

IF $\mathbf{n}(i)^T \mathbf{k}(i) > 0 \wedge \text{uni.}$ THEN (88)

IsOn(i) = 0 (89)

ELSEIF $(\mathbf{n}(i)^T \mathbf{k}(i))(\mathbf{n}(i)^T (\mathbf{k}(i) + \mathbf{e}(i))) < 0$
 \wedge IsOn($i - 1$) = 0 THEN (90)

IsOn(i) = N_{wait} (91)

ELSE (92)

IsOn(i) = $\max(0, \text{IsOn}(i - 1) - 1)$ (93)

END IF (94)

ELSEIF $(\mathbf{n}(i)^T \mathbf{k}(i))(\mathbf{n}(i)^T (\mathbf{k}(i) + \mathbf{e}(i))) < 0$
 \wedge $\|\mathbf{q}(i) - \mathbf{p}^*(i)\| > F/\kappa$ THEN (95)

IsOn(i) = $1 + N_{\text{wait}}$ (96)

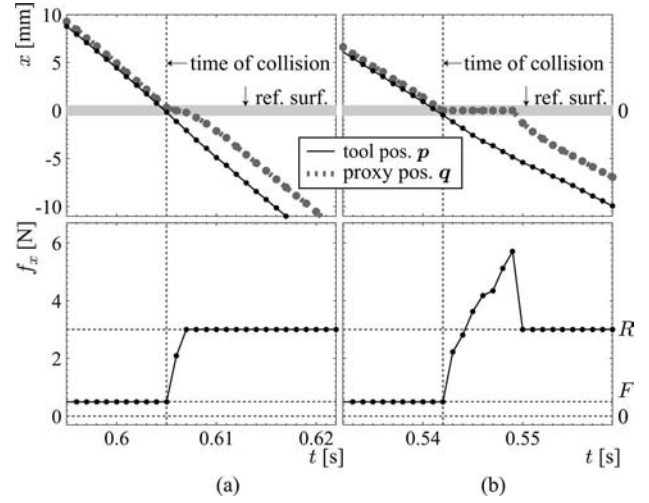


Fig. 14. Effect of N_{wait} in impedance-type implementation. (a) $N_{\text{wait}} = 0$. (b) $N_{\text{wait}} = 5$.

ELSE (97)

IsOn(i) = IsOn($i - 1$) (98)

END IF (99)

IF IsOn(i) > 0 THEN (100)

$\mathbf{q}(i) := \operatorname{argmin}_{\mathbf{r} \in \mathcal{C}} \|\mathbf{r} - \mathbf{q}(i)\|$ (101)

END IF. (102)

The aforementioned algorithm is obtained by replacing (77), “IsOn(i) = FALSE,” by the procedure of (88)–(94). The Boolean variables IsOn(i) is redefined as an integer variable here. The constant N_{wait} is a nonnegative integer. Setting $N_{\text{wait}} = 0$ reduces the algorithm into its original version (75)–(85). The integer constant N_{wait} must be equal to or larger than 2 to prevent penetrations in the admittance-type implementation because the input position $\mathbf{p}^*(i)$ depends on the proxy position of two steps ago as is apparent in (28).

The modified control algorithm (86)–(102) was demonstrated through simple experiments. The two haptic devices introduced in the previous section were used again. The reference surface \mathcal{C} was chosen as a flat surface of $x = 0$ and the fixture was chosen to be bilateral. Comparisons were performed between two values, 0 and 5, of the parameter N_{wait} with the other parameters (such as T , K , B , M , R , and F) being the same as those in the previous section. The value $N_{\text{wait}} = 5$ was chosen by trial and error so as to distinctly demonstrate the effect of this parameter. The tools were moved toward \mathcal{C} and were pushed to penetrate \mathcal{C} intentionally. The results are shown in Figs. 14 and 15. With $N_{\text{wait}} = 5$, in both types of implementation, the proxy stayed on \mathcal{C} for several time steps, and as a consequence, an impulsive force higher than the yield force was produced. These results suggest that the modified algorithm can be useful for preventing unintended postimpact penetrations and, as a beneficial side effect, to present a distinct perception of collision with \mathcal{C} .

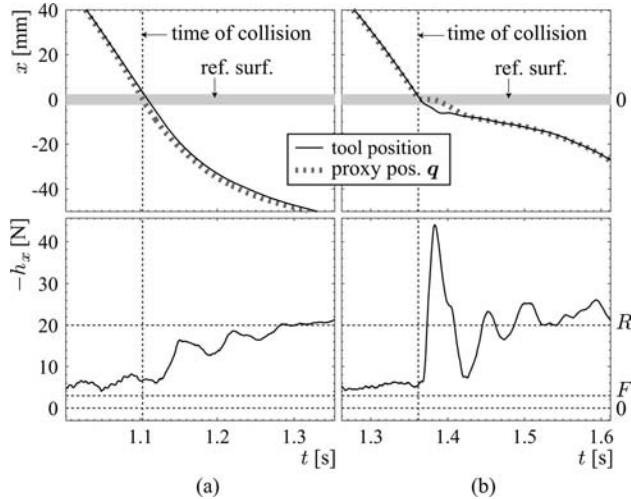


Fig. 15. Effect of N_{wait} in admittance-type implementation. (a) $N_{\text{wait}} = 0$. (b) $N_{\text{wait}} = 5$.

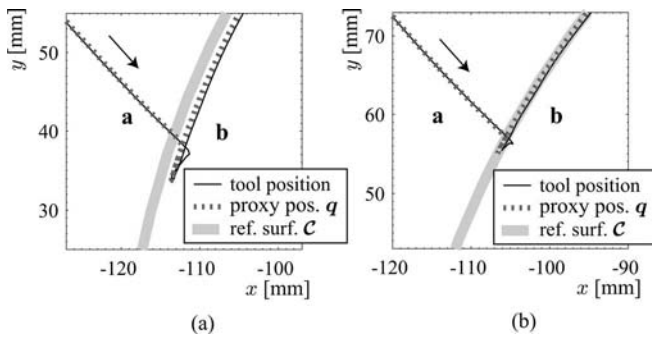


Fig. 16. Effect of N_{wait} in admittance-type implementation with a circular reference surface. Note that (a) is a duplicate of Fig. 11(b, left) for comparison. (a) $N_{\text{wait}} = 0$. (b) $N_{\text{wait}} = 15$.

Another experiment was performed to demonstrate the modified control algorithm (86)–(102) in combination with a curved reference surface in the situation identical to that of Fig. 11 except $N_{\text{wait}} = 15$. Fig. 16 shows the comparison between the data with $N_{\text{wait}} = 0$, which is the duplicate of Fig. 11(b, left), and the newly obtained data with $N_{\text{wait}} = 15$. It apparently demonstrates that the penetration was prevented by using a nonzero N_{wait} . Nevertheless, the penetration depth also depends on the user's motion and force. A quantitatively optimal choice of the parameter N_{wait} is left outside the scope of this paper, which will require experiments involving human participants. Obviously a much larger N_{wait} value (for example, $N_{\text{wait}} > 1000$ with $T = 0.001$ s) will produce some unnatural feeling because the user will feel a sudden loss of resistance after a few seconds of waiting to enter a nonpreferred region. An appropriate duration time of an impulsive force that is felt as a natural “detent” might have to be sought to determine an appropriate value for N_{wait} .

VI. CONCLUSION

This paper has presented a control framework for producing virtual fixtures that normally act as hard walls but allow intended

penetration without storing elastic potential energy. The core idea is the use of simulated position-dependent anisotropic plasticity. The plasticity-based virtual fixtures are expected to be intrinsically safer than energy-storing (e.g., elastic) fixtures. Also, they are expected to have an advantage over viscosity-based virtual fixtures [9], [11], [12] in that the user can recognize nonpreferred directions by pushing the tool with forces smaller than a predetermined yield force, without actually penetrating it. This paper has provided control algorithms for producing plasticity-based virtual fixtures by utilizing a recently proposed technique [15] to deal with discontinuous nature of plasticity in discrete-time systems. The proposed control algorithms were demonstrated through implementation experiments using admittance-type and impedance-type haptic devices. Besides, a modified algorithm was presented to prevent unintended penetrations caused by collision impacts.

The techniques established in this paper will allow empirical evaluation of the effects of the plasticity-based virtual fixtures onto the human performance of precise manual tasks. Empirical comparisons to conventional approaches will be necessary to provide quantitative support and to clarify in what specific situations the proposed approach is beneficial. Besides, the optimization of the parameters should be investigated. Although K , B , and M can be chosen depending on the control bandwidth of the haptic device to be used, optimization of the choice of R , F , and N_{wait} will need careful experiments involving human participants under some specific tasks. It will also be possible to consider further variations of the geometry of the set $\mathcal{A}(\mathbf{p}^*(i))$.

The use of the proposed method in telemanipulation will not be difficult. It may, however, need some clarifications with considering the difference in whether the virtual fixture is defined on the master's side or slave's side, which has been investigated in [8]. Moreover, further mathematical sophistications will be necessary to incorporate a reference surface \mathcal{C} of less than $n - 1$ dimension, such as a one-dimensional surface (a curve) in three-dimensional space and a zero-dimensional surface (a point) in two- or three-dimensional space.

ACKNOWLEDGMENT

The authors would like to thank the engineers at Toyota Motor Corporation who motivated this study. They are also grateful to the anonymous reviewers who provided constructive suggestions particularly concerning the passivity.

REFERENCES

- [1] R. Kikuuwe, N. Takesue, and H. Fujimoto, “Passive virtual fixtures based on simulated position-dependent anisotropic plasticity,” in *Proc. IEEE Int. Conf. Robot. Autom.*, 2007, pp. 3263–3268.
- [2] T. Sato and S. Hirai, “Language-aided robotic teleoperation system (LARTS) for advanced teleoperation,” *IEEE J. Robot. Autom.*, vol. RA-3, no. 5, pp. 476–481, Oct. 1987.
- [3] L. B. Rosenberg, “Virtual fixtures: Perceptual tools for telerobotic manipulation,” in *Proc. Virtual Reality Annu. Int. Symp.*, 1993, pp. 76–82.
- [4] S. Park, R. D. Howe, and D. F. Torchiana, “Virtual fixtures for robotic cardiac surgery,” in *Proc. 4th Int. Conf. Med. Image Comput. Comput.-Assisted Intervention*, 2001, pp. 1419–1420.
- [5] S. Payandeh and Z. Stanisic, “On application of virtual fixtures as an aid for telemanipulation and training,” in *Proc. 10th Symp. Haptic Interfaces Virtual Environ. Teleoperator Syst.*, 2002, pp. 18–23.

- [6] J. J. Abbott and A. M. Okamura, "Virtual fixture architectures for telemanipulation," in *Proc. IEEE Int. Conf. Robot. Autom.*, 2003, pp. 2798–2805.
- [7] H. Kang, Y. S. Park, T. F. Ewing, E. Faulring, and J. E. Colgate, "Visually and haptically augmented teleoperation in D&D tasks using virtual fixtures," in *Proc. Amer. Nuclear Soc. 10th Int. Conf. Robot. Remote Syst. Hazardous Environ.*, 2004, pp. 466–471.
- [8] J. J. Abbott and A. M. Okamura, "Stable forbidden-region virtual fixtures for bilateral telemanipulation," *Trans. ASME: J. Dyn. Syst., Meas., Control*, vol. 128, pp. 53–64, 2006.
- [9] J. J. Abbott and A. M. Okamura, "Pseudo-admittance bilateral telemanipulation with guidance virtual fixtures," *Int. J. Robot. Res.*, vol. 26, pp. 865–884, 2007.
- [10] C. A. Moore, M. A. Peshkin, and J. E. Colgate, "Cobot implementation of virtual paths and 3-D virtual surfaces," *IEEE Trans. Robot. Autom.*, vol. 19, no. 2, pp. 347–351, Apr. 2003.
- [11] P. Marayong, M. Li, A. M. Okamura, and G. D. Hager, "Spatial motion constraints: Theory and demonstrations for robot guidance using virtual fixtures," in *Proc. IEEE Int. Conf. Robot. Autom.*, 2003, pp. 1954–1959.
- [12] A. Bettini, P. Marayong, S. Lang, A. M. Okamura, and G. D. Hager, "Vision-assisted control for manipulation using virtual fixtures," *IEEE Trans. Robot.*, vol. 20, no. 6, pp. 953–966, Dec. 2004.
- [13] H. C. Lin, P. Marayong, K. Mills, R. Karam, P. Kazanzides, A. M. Okamura, and G. D. Hager, "Portability and applicability of virtual fixtures across medical and manufacturing tasks," in *Proc. IEEE Int. Conf. Robot. Autom.*, 2006, pp. 225–231.
- [14] G. Srimathveeravalli, V. Gourishankar, and K. Thenkurussi, "Comparative study: Virtual fixtures and shared control for rehabilitation of fine motor skills," in *Proc. 2nd Joint Eurohaptics Conf. Symp. Haptic Interfaces Virtual Environ. Teleoperator Syst. (World Haptics Conf. 2007)*, pp. 304–309.
- [15] R. Kikuuwe, N. Takesue, A. Sano, H. Mochiyama, and H. Fujimoto, "Admittance and impedance representations of friction based on implicit Euler integration," *IEEE Trans. Robot.*, vol. 22, no. 6, pp. 1176–1188, Dec. 2006.
- [16] N. Takesue, R. Kikuuwe, A. Sano, H. Mochiyama, and H. Fujimoto, "Tracking assist system using virtual friction field," in *Proc. IEEE/RSJ Int. Conf. Intell. Robots Syst.*, 2005, pp. 2134–2139.
- [17] J. M. Brown J. E. Colgate, "Passive implementation of multibody simulations for haptic display," in *Proc. 1997 ASME Int. Mech. Eng. Congr. Exhib.*, pp. 85–92.
- [18] R. J. Adams and B. Hannaford, "Stable haptic interaction with virtual environments," *IEEE Trans. Robot. Autom.*, vol. 15, no. 3, pp. 465–474, Jun. 1999.
- [19] M. Mahvash and V. Hayward, "High-fidelity passive force-reflecting virtual environments," *IEEE Trans. Robot.*, vol. 21, no. 1, pp. 38–46, Feb. 2005.
- [20] J. J. Abbott and A. M. Okamura, "Effects of position quantization and sampling rate on virtual wall passivity," *IEEE Trans. Robot.*, vol. 21, no. 5, pp. 952–964, Oct. 2005.
- [21] N. Diolaiti, G. Niemeyer, F. Barbagli, and J. K. Salisbury, "Stability of haptic rendering: Discretization, quantization, time delay, and Coulomb effects," *IEEE Trans. Robot.*, vol. 22, no. 2, pp. 256–268, Apr. 2006.
- [22] C. B. Zilles and J. K. Salisbury, "A constraint-based God-object method for haptic display," in *Proc. IEEE/RSJ Int. Conf. Intell. Robots Syst.*, 1995, pp. 146–151.
- [23] D. C. Ruspin, K. Kolarov, and O. Khatib, "The haptic display of complex graphical environments," in *Proc. ACM SIGGRAPH 1997*, pp. 345–352.
- [24] R. Kikuuwe and H. Fujimoto, "Incorporating geometric algorithms in impedance- and admittance-type haptic rendering," in *Proc. 2nd Joint Eurohaptics Conf. Symp. Haptic Interfaces Virtual Environ. Teleoperator Syst. (World Haptics Conf. 2007)*, pp. 249–254.
- [25] C. Richard and M. R. Cutkosky, "The effects of real and computer generated friction on human performance in a targeting task," in *Proc. ASME IMECE 2000 Symp. Haptic Interfaces Virtual Environ. Teleoperator Syst.*, vol. 69, pp. 1101–1108.
- [26] R. Kikuuwe and H. Fujimoto, "Proxy-based sliding mode control for accurate and safe position control," in *Proc. IEEE Int. Conf. Robot. Autom.*, 2006, pp. 26–31.



Ryo Kikuuwe (S'02–M'03) received the B.S., M.S., and Ph.D. (Eng.) degrees from Kyoto University, Kyoto, Japan, in 1998, 2000, and 2003, respectively, all in mechanical engineering.

From 2003 to 2007, he was an Endowed-Chair Research Associate at Nagoya Institute of Technology, Nagoya, Japan. He is currently an Associate Professor at Kyushu University, Fukuoka, Japan. His current research interests include human–robot coordination, real-time simulation for haptic rendering and physics-based animation, and tactile sensing.

Prof. Kikuuwe is a member of the Robotics Society of Japan, the Japan Society of Mechanical Engineers, the Society of Instrument and Control Engineers (Japan), and the Virtual Reality Society of Japan.



Naoyuki Takesue (M'02) received the B.E. and M.E. degrees in mechanical and control engineering from the University of Electro-Communications, Tokyo, Japan, in 1995 and 1997, respectively, and the Ph.D. degree in mechanical engineering from Osaka University, Osaka, Japan, in 2000.

During 2000–2003, he was a Research Associate at Osaka University. In 2003, he was an Assistant Professor at Nagoya Institute of Technology, Nagoya, Japan, where he was an Associate Professor in 2005. Since 2008, he has been an Associate Professor at

Tokyo Metropolitan University, Tokyo. His current research interests include design and motion control of mechanical systems, human–machine interface, haptics, and flexible robots.

Dr. Takesue was a Research Fellow of the Japan Society for the Promotion of Science from 1997 to 2000.



Hideo Fujimoto received the B.E. and Dr. Eng. degrees in mechanical engineering from Nagoya University, Nagoya, Japan, in 1970 and 1982, respectively.

He is currently a Professor in the Graduate School, Nagoya Institute of Technology, Nagoya, Japan, where he is also the Director of the Quality Innovation Techno-Center. His current research interests include medical engineering, haptic engineering, and robotics.

Prof. Fujimoto is a Fellow and a Councilor of the Japan Society of Mechanical Engineers and the Chairperson of Aichi Prefecture Manufacturing Personnel Training Meeting. He was a member of the Committee on Cultural Resources of the Council for Science and Technology of the Ministry of Education, Culture, Sports, Science and Technology of Japan and the President of the Scheduling Society of Japan. He was the recipient of the Best Paper Award for a paper presented at the Japan–USA Flexible Automation Symposium 2000, the Best Paper Award at the 6th Robotics Symposium, the Contribution Award from the System Integration Section, Society of Instrument and Control Engineers, and the Great Contribution Award from the Production System Section, and the Japan Society of Mechanical Engineers in 2002.